Pharmacogn J. 2026; 18(2): 171-180
A Multifaceted Journal in the field of Natural Products and Pharmacognosy
www.phcogj.com

Original Article

Design and Virtual Screening of Dihydropyrimidinone and Chromene-Based Derivatives as Potential SARS-CoV-2 NSP16 Methyltransferase Inhibitors

Dinar Adriaty[1,4], Hery Suwito[2,3]*, Ni Nyoman Tri Puspaningsih[2,3]*

ABSTRACT

Background: Dihydropyrimidinone (DHPM) and chromene scaffolds are widely recognized as bioactive heterocyclic frameworks frequently found in natural products and known for their structural versatility and synthetic accessibility. Numerous studies have reported diverse pharmacological activities of DHPM and chromene derivatives, including antiviral properties. In our preliminary study, representative DHPM and chromene derivatives, S12 and S10, exhibited antiviral activity against SARS-CoV-2 in cell-based assays (IC_{50} = 6.187–8.52 μM), supporting further structural optimization. **Objective:** This study aimed to perform structure-based virtual screening of DHPM and chromene derivatives based on two antiviral lead compounds identified in our preliminary study (S12 and S10) targeting the SARS-CoV-2 nonstructural protein 16 (NSP16), a 2′-O-methyltransferase involved in viral RNA capping and immune evasion. **Materials and Methods:** A library of 503 designed derivatives and eight repurposed antiviral drugs as reference compounds were screened against NSP16 (PDB ID: 8F4S). Compound ranking was performed using a Selection Score (SS) integrating docking score, docking pose quality, and predicted pharmacokinetic and toxicity parameters. Consensus docking analysis using DOCK6 and AutoDock Vina was applied to improve the robustness of compound ranking. **Results:** Several derivatives demonstrated favorable binding interactions within the NSP16 cryptic pocket and acceptable predicted ADMET profiles. Cross-platform docking comparison showed moderate ranking agreement between the two docking engines, supporting the robustness of the prioritization process within a computational framework. **Conclusion:** Based on the integrated virtual screening approach, two DHPM and one chromene derivatives were identified as prioritized candidates for SARS-CoV-2 NSP16 inhibition and can be further evaluated in experimental studies.

Keywords: allosteric inhibition; consensus docking; cryptic pocket; methyltransferase; SARS-CoV-2

Dinar Adriaty[1,4], Hery Suwito[2,3]*, Ni Nyoman Tri Puspaningsih[2,3]

[1]*Doctoral Program of Mathematics and Natural Sciences, Faculty of Science and Technology, Universitas Airlangga, MERR-C Mulyorejo, Surabaya – 60115, East Java, INDONESIA.*

[2]*Department of Chemistry, Faculty of Science and Technology, Universitas Airlangga, MERR-C Mulyorejo, Surabaya – 60115, East Java, INDONESIA.*

[3]*UCoE Research Center for Bio-Molecule Engineering, (BIOME), Universitas Airlangga, MERR-C Mulyorejo, Surabaya – 60115, East Java, INDONESIA.*

[4]*Research Center on Global Emerging and Re-emerging Infectious Diseases (RC-GERID), Institute of Tropical Disease, Universitas Airlangga, MERR-C Mulyorejo, Surabaya – 60115, East Java, INDONESIA.*

Correspondence

S. Hery

Department of Chemistry, Faculty of Science and Technology, Universitas Airlangga, MERR-C Mulyorejo, Surabaya – 60115, East Java INDONESIA.

E-mail: hery-s@fst.unair.ac.id

History

- Submission Date: 27-02-2026;
- Review completed: 30-03-2026;
- Accepted Date: 06-04-2026.

DOI : 10.5530/pj.2026.18.131

Article Available online

http://www.phcogj.com/v18/i2

INTRODUCTION

The coronavirus disease 2019 (COVID-19) pandemic, caused by severe acute respiratory syndrome coronavirus 2 (SARS-CoV-2), remains a major global health concern. Although vaccines and several antiviral agents have been approved, the continuous emergence of viral variants, heterogeneous immune responses, and the potential development of therapeutic resistance may reduce the long-term effectiveness of current treatments[1]. These limitations underscore the urgent need of ongoing efforts to identify and develop new antiviral candidates against SARS-CoV-2[2]. Currently, several antiviral treatments such as remdesivir (intravenous nucleotide analog) are approved for hospitalized patients to reduce disease progression, paxlovid (nirmatrelvir combined with ritonavir) is authorized for use in high-risk non-hospitalized individuals, molnupiravir is another orally active antiviral used where other treatments are unsuitable or unavailable[3]. Additionally, several monoclonal antibody therapies have been developed, though their efficacy can vary with viral variant[4].

In a previous preliminary study, two small heterocyclic scaffolds derived from dihydropyrimidinone (DHPM) and chromene, demonstrated favorable pharmacological activity against SARS-CoV-2. The compounds S-10, (R)-2-amino-7-hydroxy-4-phenyl-4H-chromene-3-carbonitrile and S-12, ethyl (R)-6-methyl-2-oxo-4-phenyl-1,2,3,4-tetrahydropyrimidine-5-carboxylate, exhibited IC_{50} = 8.52 ± 0.28μM and 6.187 ± 0.41μM, respectively, in a phenotypic cell-based assay using SARS-CoV-2 infected Vero cells, where viral replication was determined by quantifying viral RNA levels using real-time PCR (RT-qPCR). Cytotoxicity was assessed using an MTT assay, and both compounds demonstrated high selectivity index (SI > 150), indicating selective antiviral activity relative to cytotoxicity[5]. Subsequent computational studies expanded these scaffolds into systematic derivatives and evaluated them against the viral main protease (Mpro) and papain-like protease (PLpro), based on ADMET properties and molecular docking profiling[6]. Candidate compounds were ranked via a selection score approach integrating drug-likeness parameters and docking metrics relative to reference drugs[7].

As SARS-CoV-2 replication depends on multiple essential viral enzymes, expanding scaffold evaluation toward additional viral proteins may enhance the probability of identifying compounds with broader antiviral relevance. Targeting multiple essential enzymes involved in distinct stages of the viral life cycle, including proteolytic processing and RNA maturation, may contribute to integrated antiviral development strategies and potentially reduce vulnerability to resistance. Building on these

Cite this article: Dinar A, Hery S, Ni N T P. Design and Virtual Screening of Dihydropyrimidinone and Chromene-Based Derivatives as Potential SARS-CoV-2 NSP16 Methyltransferase Inhibitors. Pharmacogn J. 2026;18 (2): 171-180.

findings, the present study extends the evaluation of DHPM and chromene derivatives to nonstructural protein 16 (NSP16) that essential for viral RNA capping process[8]. NSP16 is the 2′-O-methyltransferase or 2′-O-MTase, responsible for forming the cap-1 structure on viral mRNA, a modification required for RNA stability and evasion of host innate immunity[9]. The enzyme utilizes S-adenosyl methionine (SAM) as its natural methyl donor, and most classical inhibition strategies have therefore focused on the SAM-binding site or on sinefungin-based competitive inhibition. However, this canonical catalytic pocket is highly conserved among human methyltransferases, which reduces selectivity and increases the potential for off-target interactions[10].

Unlike most previous studies that focus on the SAM-binding catalytic site of NSP16, the present study specifically targets a recently identified cryptic allosteric pocket. Currently, structure-based virtual screening of DHPM and chromene derivatives directed toward this cryptic site has not been extensively explored. Therefore, this approach provides a distinct strategy for identifying potential non-competitive inhibitors with improved selectivity. A recent crystallographic study by Inniss et al. (2024) reported the presence of a previously hidden cryptic allosteric pocket adjacent to the SAM-binding cleft (PDB ID: 8F4S). This pocket becomes accessible through localized conformational rearrangements and can accommodate small molecules that interfere cryptically with SAM positioning. Targeting this alternative site may offers advantages, including potential improved in selectivity, avoidance of direct SAM competition, and access to a more flexible binding region compared with the rigid canonical active site[11].

The observation focuses on predicting the binding of DHPM[12] and chromene[13] derivatives to the cryptic allosteric pocket of NSP16 to identify a potential non-classical inhibition mechanism. These compounds are known to be easily varied and modified based on their constituent components, yet their activity against SARS-CoV-2 remains largely unexplored. To explore this opportunity, DHPM and chromene scaffolds were further systematically modified by adding 14 electronic and steric substituents forming a compound library for structure-based virtual screening. The selection of substituents was based on their well-established roles in modulating electronic and steric properties in medicinal chemistry. Electron-donating and electron-withdrawing groups were systematically introduced to influence hydrogen-bonding capacity, polarity, and hydrophobic interactions. These modifications were intended to enhance ligand compatibility with the NSP16 cryptic pocket, particularly by optimizing interactions with key residues identified in the crystallographic structure[14].

The database was developed and subsequently applied in virtual screening to identify compounds with improved 2′-O-MTase inhibition potential and reduced toxicity. Castro-Gonzalez et al. (2020) introduced a selection score (SS) model that evaluates drug candidates by integrating ADMET parameters to determine drug-likeness and toxicity. The model also utilizes docking-based parameters, including docking scores and pharmacophore-related pose quality, to assess the suitability of each compound through predicted receptor–ligand interactions[15]. In response to recognized variability among docking algorithms, a comparative consensus docking strategy was implemented by employing independent docking programs to cross-validate binding predictions. This approach was implemented to reduce scoring bias and improve confidence in compound prioritization within a virtual screening workflow.

To address potential variability among docking algorithms, a comparative consensus docking strategy was implemented using two independent docking engines, DOCK6 and AutoDock Vina. This approach was adopted to enhance ranking consistency and reduce scoring bias at the virtual screening stage. Docking calculations were independently conducted using DOCK6 and AutoDock Vina under validated protocols. Rather than relying on a single scoring function, compound prioritization was based on comparative ranking consistency between the two docking engines[16]. This cross-validation strategy was employed to improve the robustness of compound selection within the scope of the present virtual screening study[17].

Therefore, the present study aims to conduct structure-based virtual screening of dihydropyrimidinone (DHPM) and chromene derivatives against the NSP16 cryptic pocket by integrating a comparative consensus docking strategy with a selection score based ranking system. The selection score combines docking energy, dock pose interaction parameters, predicted ADME properties, and toxicity estimations to support systematic compound ranking. Through cross-platform validation using DOCK6 and AutoDock Vina, this integrated approach enhances ranking robustness and supports the identification of computationally prioritized candidates for subsequent experimental evaluation.

MATERIALS AND METHODS

Materials

The SARS-CoV-2 2'-O-Methyltransferase is crystallized in complex with compound 4-[(E)-2-(2,4-dichlorophenyl)ethenyl]-6-(trifluoromethyl) pyrimidin-2-ol (5a) bound to the cryptic pocket of NSP16 (PDB ID: 8F4S, resolution 2.15 Å)[11]. All structural data were retrieved from the RCSB Protein Data Bank website http://www.rcsb.org/pdb. The eight repurposed drugs chosen were Lopinavir, Remdesivir, Indinavir, Ritonavir, Molnupiravir, Favipiravir, Ensitrelvir, and Nirmatrelvir, selected as reference drugs for their well-established safety profiles. Reference drug structures taken from the website https://pubchem.ncbi.nlm.nih.gov. A total of 503 DHPM and Chromene derivatives were developed as chemical database candidates derived from two different small molecule scaffolds.

Instrumentation

Molecular docking analysis was conducted using software tools on both Windows 11 and Linux operating systems. The software used on the Windows system includes ChemDraw Professional 15.1, Notepad++, Chimera 1.16, PuTTY (64-bit), WinSCP, PyMol software v2.4.1 (Schrödinger, Inc, USA) and Discovery Studio Visualizer (BIOVIA, San Diego) 2021 v21.1.0.2098. On the LINUX system, Gaussian 16 was used for optimizations of the 3D structures and DOCK6 Program. Autodock Vina (PyRx 0.8 software) was utilized for consensus molecular docking. The 3D structures were drawn using the tool available at https://cactus.nci.nih.gov/translate/, while the prediction of ADMET (Absorption, Distribution, Metabolism, Excretion and Toxicity) of candidate ligands was conducted using the SwissADME web service and software T.E.S.T (Toxicity Estimation Software Tool) for assessing toxicity and mutagenicity.

Compound library preparation

Two scaffold compounds that had previously shown in vitro test of antiviral activity against SARS-CoV-2, one dihydropyrimidinone (DHPM) and one chromene derivative, were used as lead compounds. A total of 503 derivatives were generated by introducing 14 substituents (-OH, -OCH_3, -OCH_2CH_3, -F, -Cl, -Br, -I, -NO_2, -NH_2, -CH_3, -CH_2CH_3, -CN, -$N(CH_3)_2$, and -$N(CH_2CH_3)_2$) at various positions on the aromatic ring. Ligands were drawn in ChemDraw, converted to SMILES, and 3D structures were generated via the NIH CACTUS translator (https://cactus.nci.nih.gov/translate/) in sdf format. Geometry optimization was performed using the semi-empirical PM6 method in Gaussian 16, and partial charges were assigned using the AM1-BCC approach via the Antechamber module. All ligands were saved in MOL2 format for subsequent docking. For AutoDock Vina

docking, ligands were imported into PyRx software, where they were converted to PDBQT format and Gasteiger charges were automatically assigned according to the AutoDock Vina protocol[18,19].

Receptor preparation

For DOCK6 calculations, the NSP16 structure (PDB ID: 8F4S) was preprocessed using DockPrep in UCSF Chimera. Water molecules, ions, and non-essential heteroatoms were removed. Polar hydrogens and charges were added using the ff14SB force field for the protein and AM1-BCC for non-protein components. The DMS (Dot Molecular Surface) file was generated to map the receptor surface, followed by SPHGEN for sphere generation[20]. Spheres within an 8 Å radius from the original ligand 5a were retained using sphere selector, defining the active site region within the cryptic pocket.

For AutoDock Vina calculations, the NSP16 structure (PDB ID: 8F4S) was prepared from the same preprocessed structure used for DOCK6 to ensure methodological consistency. Structural inspection and removal of non-essential heteroatoms were performed in PyMol. The protein was then converted to PDBQT format using AutoDockTools, where polar hydrogens were added and Gasteiger charges were assigned according to Vina requirements[18]. The docking grid box was centered on the cryptic pocket defined by the co-crystallized ligand 5a, using dimensions comparable to those applied in DOCK6[21].

Residue numbering was verified by global sequence alignment of the 8F4S chain A with the NSP16 region of the SARS-CoV-2 ORF1ab polyprotein (UniProt: P0DTD1) using the EMBOSS Needle pairwise alignment tool (https://www.ebi.ac.uk/jdispatcher/psa/emboss_needle). The alignment showed identical sequences without gaps, confirming that residues 6799–7096 in the crystallographic structure correspond directly to positions 1–298 in the renumbered docking model. Based on this alignment, a consistent numbering conversion was applied throughout the study, allowing accurate mapping of reported residues between numbering schemes; key residues described by Inniss et al. (2024) correspond to Thr120, Lys160, Phe156, Leu111, Met131, and Ile153 in the docking model.

Molecular Docking

For DOCK6 calculations, geometry-optimized ligands were saved in MOL2 format with AM1-BCC partial charges assigned using the Antechamber module[22]. The flexible docking protocol in DOCK6 was validated by redocking the native ligand (5a), with reliability confirmed by achieving an RMSD ≤ 2 Å, following the criteria established by Allen et al. (2015)[21]. After validation, 503 designed DHPM and chromene derivatives, along with 8 reference compounds, were docked into the NSP16 receptor. Compounds meeting docking reliability criteria were selected for further analysis in the results section.

For AutoDock Vina calculations, the same ligand structures were imported into PyRx (version 0.8) and converted to PDBQT format, where polar hydrogens were added and Gasteiger partial charges were assigned according to the AutoDock Vina protocol [18]. Rotatable bonds were automatically defined during PDBQT conversion.

Comparative Consensus Docking Analysis

Binding affinity alone was not considered sufficient for compound selection. Docking scores represent simplified approximations of protein–ligand interactions and do not fully capture the complexity of real molecular recognition processes, as they inherently neglect factors such as protein flexibility, solvent effects, and entropic contributions. Consistent with the integrated virtual screening strategy proposed by Gónzalez et al., 2020 compound selection was therefore based on a composite selection score incorporating docking pose reliability, interaction consistency with key binding-site residues, and predicted ADMET properties[23]. This integrated scoring approach allows simultaneous evaluation of multiple parameters and reduces the risk of prematurely discarding promising compounds that might occur in sequential screening workflows, where filters such as toxicity or docking score are applied stepwise. Combining these criteria into a single composite metric allows compounds to be prioritized based on their overall balance of binding performance and pharmacokinetic properties rather than on a single parameter alone.

The 503 derivatives were initially screened using DOCK6 and compounds were ranked based on the calculated selection score (SS). Compounds were sorted in descending order of total SS to generate the primary ranking list. The top 50 ranked compounds were subsequently reevaluated using AutoDock Vina. For this stage, the same selection score framework was applied, with docking related components derived from AutoDock Vina results while retaining identical ADME and toxicity parameters. Compounds were again ranked according to total SS values generated from Vina-derived docking results.

Ranking consistency between DOCK6 based SS and AutoDock Vina based SS was assessed by comparing ranking positions (ΔRank) for each compound and calculating the Spearman rank correlation coefficient (ρ) across the top 50 compounds. Spearman analysis was selected to evaluate directional agreement between the two ranking systems without assuming linear correlation. Overlap percentage among top-ranked compounds was also determined to quantify cross-platform convergence[24].

Analysis of ADMET Predictions

Drug-likeness evaluation was conducted using SwissADME, based on Lipinski's Rule of Five and additional criteria (Ghose, Veber, Egan, and Muegge)[25]. Toxicity, LD_{50} (mg/kg), and Ames mutagenicity (M) were assessed using Toxicity Estimation Software Tool (T.E.S.T) program[26]. ADMET scoring was performed according to predefined acceptance criteria for each evaluated parameter. Each criterion was assigned a binary score (1 = fulfilled; 0 = not fulfilled), and total ADMET scores were calculated for each compound. These values were subsequently compared with those of the reference drugs for relative assessment. The use of multiple reference drugs minimized bias associated with single-compound dependence and enabled a more robust discrimination of ligands with realistic pharmacological relevance[27].

RESULT AND DISCUSSION

Design of 2′-O-methyltransferase inhibitors

A total of 503 derivatives were obtained by introducing 14 electron-donating and electron-withdrawing substituents have been widely employed in Hammett–Hansch substituent studies at various aromatic positions to explore structure–activity relationships[28] as described in Table 1, which illustrates the scaffold modification and substituent placement strategy. Substituent placement was performed using a two-stage design. In the first stage, single substitution was introduced at different positions on the B ring. In the second stage, identical disubstitution was applied at selected position pairs (R1–R4). Each positional variant was treated as a distinct compound to account for positional effects on the B ring. Design strategy aimed to refine hydrogen-bond donor and acceptor features, strengthen π–π interactions, and modulate molecular polarity to improve compatibility with the binding pocket of the viral 2′-O-methyltransferase (NSP16).

Dihydropyrimidinone (DHPM) and chromene scaffolds were selected as starting points of exploration because both exhibit chemical features that are frequently associated with antiviral potential. DHPM derivatives, as representatives of Biginelli-type heterocyclic, can originate from natural sources or be obtained through synthetic

Table 1. Variation Candidate Compounds

Code	Structure and Name of Compound (IUPAC)	Substituents	
		Position on B Ring	Potential Functional group
S-12	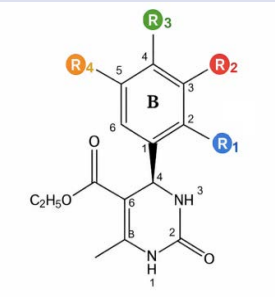	Single subtitution, Different position C2-R1 C3-R2 C4-R3 C5-R4	R1 -OH, -OMe, -OEt, -Me, -Et, -F, -Cl, -Br, -I, $-NO_2$, $-NH_2$, -CN, $-N(Me)_2$, $-N(Et)_2$ R2 -OH, -OMe, -OEt, -Me, -Et, -F, -Cl, -Br, -I, $-NO_2$, $-NH_2$, -CN, $-N(Me)_2$, $-N(Et)_2$ R3 -OH, -OMe, -OEt, -Me, -Et, -F, -Cl, -Br, -I, $-NO_2$, $-NH_2$, -CN, $-N(Me)_2$, $-N(Et)_2$
	IC_{50} = 6.187 ± 0.41 µM ethyl (*R*)-6-methyl-2-oxo-4-phenyl-1,2,3,4-tetrahydropyrimidine-5-carboxylate		
S-10	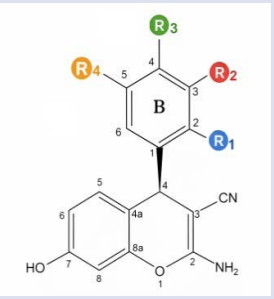	Identical disubstitution, Different position C2,C3-R1,R2 C2,C4-R1,R3 C3,C4-R2,R3 C3,C5-R2,R4	R4 -OH, -OMe, -OEt, -Me, -Et, -F, -Cl, -Br, -I, $-NO_2$, $-NH_2$, -CN, $-N(Me)_2$, $-N(Et)_2$
	IC_{50} = 8.52 ± 0.28 µM (*R*)-2-amino-7-hydroxy-4-phenyl-4*H*-chromene-3-carbonitrile		

approaches, including based on green chemistry methods such as modified Biginelli reactions. It also recognized as nucleobase analogs with activity against viral polymerases and proteases[6]. DHPM and pyrimidine compounds are known for their pharmacophoric flexibility, hydrogen-bonding capacity, and broad bioactivity profiles, including emerging antiviral relevance reported in recent medicinal chemistry evaluations[29].

Chromene-based structures, particularly benzopyran and flavonoid-related scaffolds, possess conjugated aromatic systems that favor hydrophobic contacts and π–π stacking interactions commonly involved in viral protein recognition. Several chromene and flavonoid analogues have been reported since 2020 to inhibit SARS-CoV-2 in computational and biochemical assays[13]. In our previous SARS-CoV-2 antiviral assays, representatives from both DHPM and chromene classes displayed a good inhibition of SARS-CoV-2 replication[6], supporting their suitability as core scaffolds for further optimization toward targeting the viral 2′-O-methyltransferase (NSP16).

Docking validation analysis

The docking validation was performed by re-docking the native ligand 5a into the viral 2′-O-methyltransferase (NSP16) structure (PDB ID: 8F4S). During docking preparation, NSP10 was removed from the NSP16–NSP10 complex because the cryptic pocket targeted in this study is formed entirely within the NSP16 domain and does not involve residues contributed by NSP10[11]. Structural analyses have shown that NSP10 primarily stabilizes the SAM-binding loop, while the geometry of distal cryptic pockets remains unchanged in its absence[30].

Spheres were generated and simulation box was centered on the active site coordinates (x = 97.081 Å, y = 11.794 Å, z = 22.845 Å), generating 2,596,608 grid points. The redocking RMSD value for ligand 5a was 1.411 Å, indicating reliable reproduction of the co-crystallized pose. The redocking experiment successfully reproduced the key non-covalent interactions previously described by Inniss et al. (2024) for the cryptic pocket of SARS-CoV-2 NSP16. In the reference crystal structure, essential stabilizing contacts, include hydrogen bonding with Thr6918 and Lys6958, π–π stacking with Phe6954, hydrophobic interactions involving Leu6909, Met6929, and Ile6951, as well as a covalent interaction with Cys6913[11].

The residue numbering according to the reference structure reflects the original ORF1ab polyprotein indexing, rather than the simplified 1–298 sequence generated during receptor preparation for docking. However, the interaction pattern observed in our docking results remains consistent with the original ligand occupying the same pocket. The redocked ligand reproduced all of these interactions and aligned closely with the crystallographic pose, confirming that both the spatial orientation and the interaction geometry within the cryptic pocket were retained. This positional agreement, together with the conservation of interaction patterns that characterize this NSP16 cryptic pocket, supports the reliability of the docking protocol for subsequent screening and evaluation of candidate ligands[31].

As presented in Figure 1, the ligands predicted to occupy the cryptic cavity are expected to interfere with NSP16 activity through an allosteric mechanism. A molecule binding in the cryptic pocket blocks the necessary conformational motions that NSP16 needs to correctly position SAM and the RNA substrate. This loss of flexibility also weakens the stabilizing interaction with NSP10. As a result, the NSP16–NSP10 complex cannot form the catalytically competent arrangement required for 2′-O-methylation. Inhibitors of the cryptic site therefore suppress methyltransferase activity allosterically, without competing with SAM [11].

The absence of a covalent interaction with Cys6913 in the redocking of the native ligand is expected, since the DOCK6 docking procedure evaluates only non-covalent binding modes and does not account for covalent bond formation within the active site (Coumar, 2021). This limitation does not affect the validity of the redocking analysis, as pose

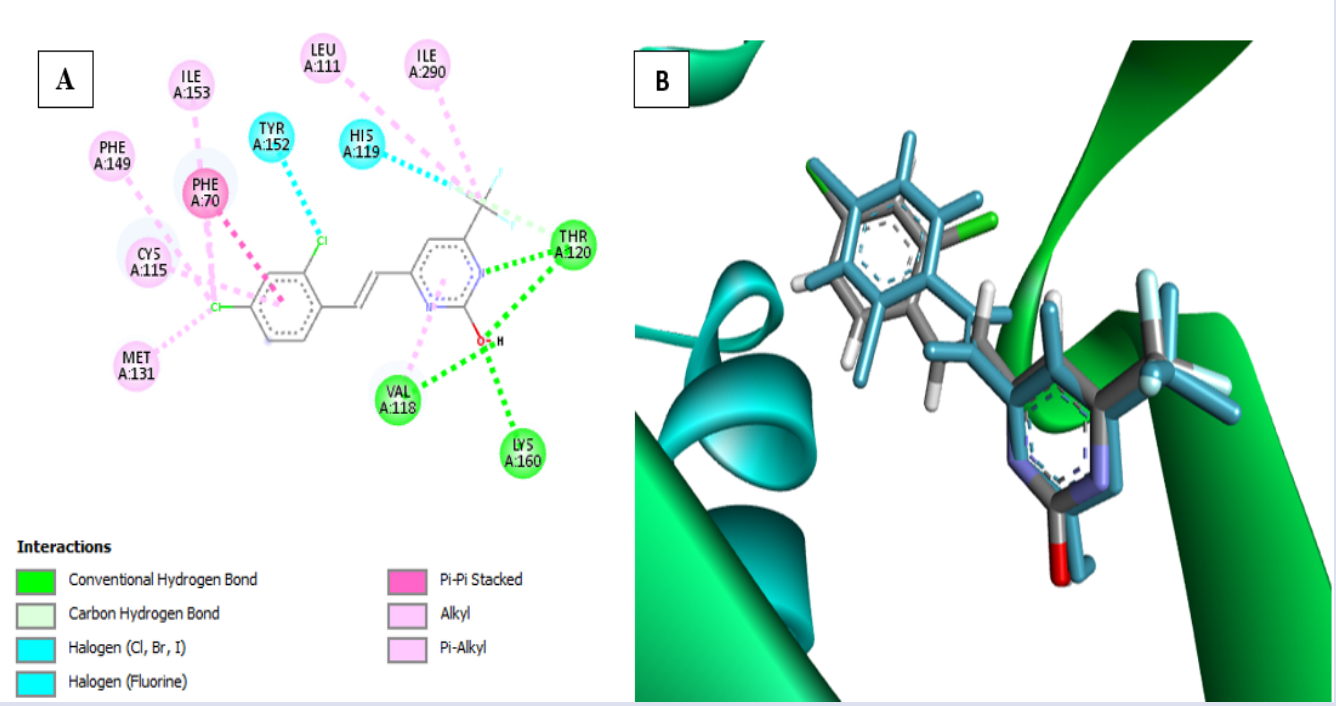

Figure 1. (**A**) 2D visualized interaction of the redocked ligand with key residues of SARS-CoV-2 NSP16 (**PDB ID: 8F4S**). (**B**) Superimposition of the native ligand (grey) and the redocked ligand (cyan) showing similar binding conformations within the cryptic site, with an RMSD value of 1.411 Å indicating a reliable redocking result (DOCK6 docking result; visualized by the Biovia Discovery Studio).

Table 2. Comparison of key binding-site interactions reported for ligand 5a in Inniss et al. (2024) with the redocking result of the native ligand (PDB ID: 8F4S) by DOCK6

Interaction Type	Residues Reported by Inniss et al. (2024)	*)Residues Observed in Redocking	Interpretation
Conventional hydrogen bond	Thr6918, Lys6958, Val6916	Thr120, Lys160, Val118	Hydrogen-bonding pattern is conserved, differences in residue numbering arise from the ORF1ab polyprotein indexing used in the 8F4S structure.
Covalent (C–S linkage)	Cys6913	Not observed	The covalent interaction cannot be reproduced because DOCK6 evaluates only non-covalent binding modes.
Hydrophobic and aromatic interactions	Phe6868, Leu6909, Met6929, Ile6951, Phe6947, Tyr6950	Phe70, Leu111, Met131, Ile153, Phe149, Tyr152	Hydrophobic and π-interactions remain conserved.

*) Residue numbering was converted using EMBOSS Needle global alignment (100% identity; publication numbering = docked numbering + 6798)

reproduction is primarily determined by the maintenance of non-covalent contacts and the overall spatial orientation of the ligand within the pocket. Although DOCK6 does not model covalent interactions and therefore cannot reproduce the covalent linkage observed between the native ligand and Cys115 (Cys6913 in ORF1ab numbering), this limitation does not affect the interpretation of binding poses within this site. In practice, several candidate compounds in our study still formed non-covalent contacts with Cys115, and proximity to this residue remains structurally meaningful (see Table 2). Cys115 is located at the base of the cryptic pocket and contributes to the local binding region described in the crystallographic reference. Thus, ligands that retain non-covalent interactions with Cys115 occupy the same sub-pocket and follow an interaction topology consistent with the experimentally validated binding mode, indicating that the docking pose is correctly positioned despite the absence of covalent bond modeling[33].

Virtual Screening Analysis

A total of 503 designed ligands and 8 reference drugs were virtually screened using DOCK6 against the validated 2′-NSP16 (O-methyltransferase) active site. A Selection Score (SS) framework was then used to combine docking scores and poses with ADME and toxicity predictions. All results were organized into a database and assessed to generate the SS values, where each criteria was scored as 1 when fulfilled and 0 when not [34]. The candidate molecules and the clinically used SARS-CoV-2 drugs were subsequently ranked based on their total SS.

The Selection Score (SS) was calculated using a composite scoring system as follows:

$$SS = (S^{FMS} + S^{T} + S^{ADME}) / N$$

Where S^{FMS} represents docking-related parameters (binding energy and pose quality), S^{T} represents average toxicity (Ames Mutagenicity and LD_{50} prediction), S^{ADME} represents ADME criteria, N represents the total number samples of evaluated parameters. Each parameter was assigned a binary value (1 = fulfilled; 0 = not fulfilled), and all parameters were equally weighted in the final score. Compounds were considered favorable if their SS values exceeded the average SS of all evaluated compounds. The SS value of the native ligand (SS = 0.6659)

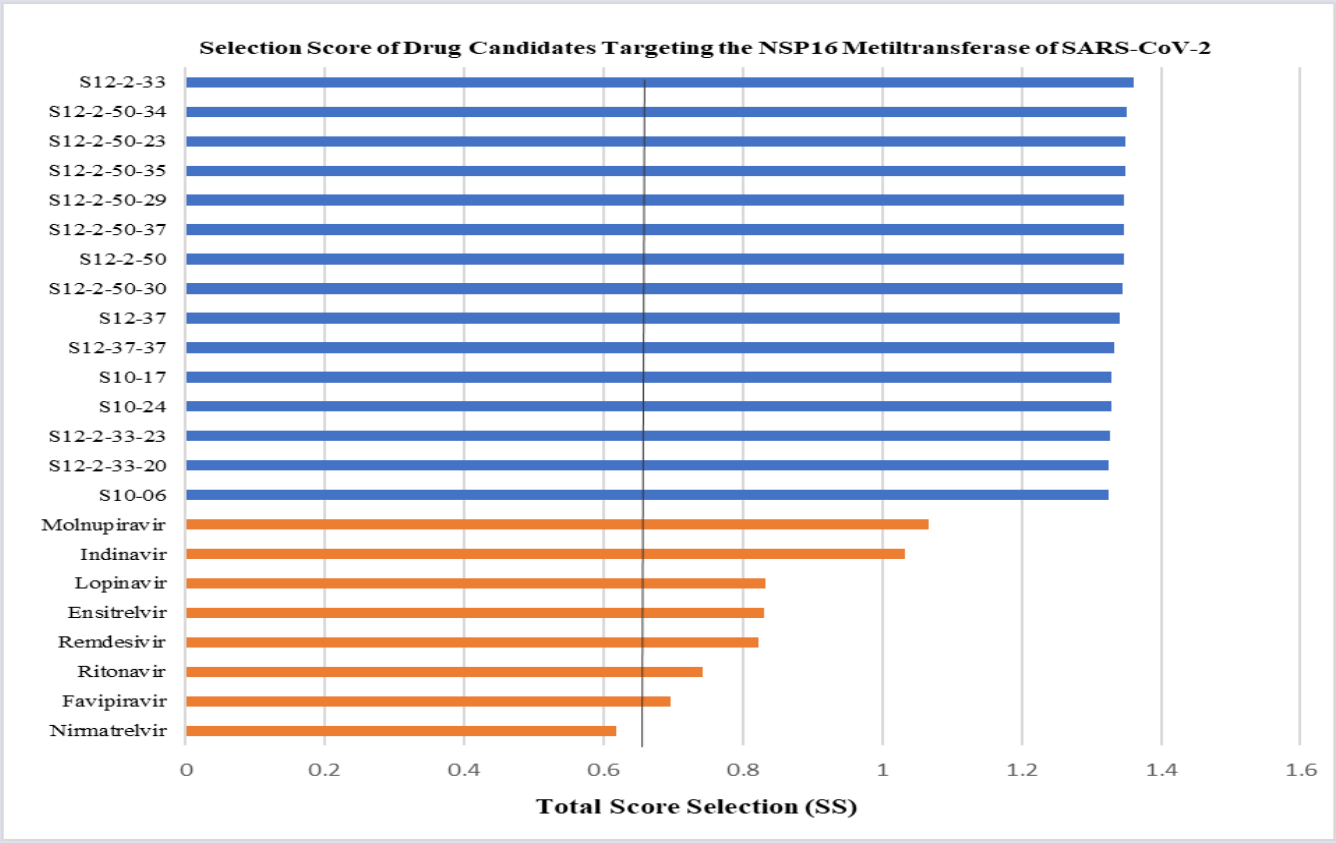

Figure 2. The Selection Score (SS) ranking of candidate ligands targeting the NSP16 SARS-CoV-2; Blue = compounds with the highest Selection Score (SS) value; Orange = Reference drugs; the vertical dashed line shows the native ligand threshold (SS = 0.6659)

Table 3. Docking Interaction Profile of Selected Compounds Against NSP16 Methyltransferase with DOCK6

Compound	Grid Score (kcal/mol)	Hydrogen Bonds	Pi Bonds and Hydrophobic Bonds
5a (original ligand)	−53.39	Thr120, Lys160, **Val118**	Phe149, Leu111, Ile153, Ile290, **Phe70**, Tyr152
S12-2-33	−44.87	**Val118**, Asp114, Cys115	**Phe70**, Met131
S12-2-50-34	−49.61	Ser98, Met131, Asp99	**Phe70**, Phe149, Leu100, Tyr152
S12-2-50-23	−46.13	Ser98, Met131, Asp99	**Phe70**, Phe149, Leu100
S12-2-50-35	-49.46	Ser98,Gly71,Met131,Asp114, Asp99	Cys115,**Phe70**,Phe156,Tyr152,Phe149,Leu100
S12-2-50-29	-48.38	Met131, Ser98,Asp99	Leu100,Phe149,Tyr152,Phe156,Cys115,Ile153, **Phe70**
S12-2-50-37	-45.95	Cys115,Phe149, Ile153,Asp114	**Phe70**,Val118,Met131,Leu100
S12-2-50	-45.27	Ser98,Met131, Asp99,Phe149	Leu100,**Phe70**,Cys115,Ile153,Tyr152
S12-2-50-30	-49.94	Met131,Gly71,Ser98,Asp114, Asp99	Phe149,Leu100,**Phe70**,Cys115,Tyr152,Phe156
S12-37	-52.76	Cys155,Phe149, Asp114	Val118,**Phe70**,met131,Leu100
S12-37-37	-48.12	Cys115 Phe149,Ile153,Asp114	Met131, Leu100,Val118, **Phe70**
S10-17	-40.33	Met131	Cys115,Val118,Leu111,Ile290,**Phe70**
S10-24	-38.95	Met131,Asp99,Cys115	**Phe70**,Phe156,Val118,1le68,Leu111,Ile290
S12-2-33-23	-45.29	**Val118**,Tyr152	Cys115,Asp114,**Phe70**,Ile153,Phe156,His119
S12-2-33-20	-45.47	**Val118**,Tyr152	Cys115,**Phe70**,Phe156,Ile153,His119
S10-06	-38.55	Tyr152,His119	**Phe70**,Cys115,Phe156,Val118,Met131

was used as a reference threshold.The full SS assessment is presented in Figure 2.

Fifteen derivative compounds were positioned among the top-ranked candidates according to the selection score, with S12-2-33 achieving the highest overall score, as presented in Table 3. Interaction analysis showed that most derivatives occupied the validated NSP16 cryptic pocket and preserved key contacts with residues identified during redocking validation, including Phe70, Cys115, Met131, Val118, Phe149, and Asp114, indicating conservation of the binding topology within the cavity. Notably, S12-2-33 formed hydrogen bonds with Val118, Asp114, and Cys115, along with hydrophobic interactions involving Phe70 and Met131, supporting a coherent binding mode within the pocket. In contrast, some higher-scoring compounds

showed interaction patterns suggestive of size-driven scoring bias or less consistent pocket engagement. Moreover, S12-2-33 exhibited a balanced physicochemical profile and a synthetically accessible chromene scaffold amenable to further structural optimization, further supporting its selection for subsequent investigation[35].

To further assess the robustness of this prioritization and minimize potential scoring-function bias associated with a single docking engine, the top-ranked compounds were subsequently re-evaluated using an independent docking platform for consensus analysis.

Comparative Consensus Docking Analysis

The top 50 compounds ranked by DOCK6-derived Selection Score (SS) were redocked using AutoDock Vina. The same receptor structure and grid box centered on the validated cryptic pocket were applied to ensure methodological consistency. Prior to large-scale screening, redocking of the native ligand was performed in AutoDock Vina under identical grid conditions, yielding an RMSD value of 2.09 Å, which confirms acceptable reproduction of the crystallographic binding pose[21]. The selection score framework was subsequently recalculated using AutodockVina derived docking energies while retaining identical ADME and toxicity components, enabling direct comparison between DOCK6 and AutoDock Vina rankings.

Ranking consistency between DOCK6 and AutoDock Vina was evaluated using ΔRank comparison and Spearman rank correlation analysis (Table 4). A statistically significant moderate positive correlation was obtained ($\rho = 0.474$, $p < 0.001$), indicating partial directional agreement between the two scoring systems. Compounds with low ΔRank values (≤5) were interpreted as demonstrating cross-platform stability, consistent with previous consensus docking studies reporting that reduced rank displacement across independent scoring functions enhances prioritization confidence (Palacio-Rodríguez et al., 2019; López-López et al., 2023).

Among the fifteen prioritized compounds, eight derivatives exhibited ΔRank ≤5, indicating stable positioning within the upper ranking tiers in both docking platforms. In contrast, several compounds showed larger rank shifts, which likely reflect sensitivity to differences in scoring formulation rather than complete loss of binding compatibility.

The observed moderate correlation ($\rho = 0.474$) indicates partial agreement between docking platforms and reflects intrinsic differences in scoring functions rather than inconsistency in ligand binding. Therefore, consensus docking should be interpreted as a strategy to improve ranking robustness rather than definitive validation of binding affinity.

Notably, S10-24 displayed identical ranking positions in DOCK6 and AutoDock Vina (ΔRank = 0). This agreement suggests consistent scoring behavior across independent search algorithms and scoring models. Structurally, S10-24 maintained hydrogen bonding with Met131, Asp99, and Cys115, together with hydrophobic contacts involving Phe70, Phe156, Val118, Leu111, and Ile290, indicating stable accommodation within the cryptic pocket.

The observed rank variations between DOCK6 and AutoDock Vina may be attributed to intrinsic differences in their scoring formulations and search algorithms. DOCK6 evaluates binding based on grid-based van der Waals and electrostatic interaction energies, emphasizing geometric complementarity within the predefined sphere cluster of the binding site[21]. In contrast, AutoDock Vina estimates binding affinity using a hybrid empirical scoring function that integrates steric, hydrophobic, hydrogen-bonding, and conformational penalty terms[18] as seen in Table 5. Because these engines rely on distinct mathematical approximations of protein–ligand interactions, differences in rank positions are expected and reflect methodological sensitivity rather than inconsistent binding behavior. Although cross-platform agreement increases confidence in computational prioritization, it does not substitute for experimental validation. Docking-based consensus should therefore be interpreted as a strategy to reduce methodological bias rather than definitive evidence of biological activity.

In summary, eight out of the fifteen prioritized compounds demonstrated cross-platform ranking stability accompanied by consistent interaction profiles within the validated NSP16 cryptic site. These derivatives may therefore be considered computationally stable candidates for subsequent experimental evaluation.

Table 4. Cross-Platform Stability of Top 15 Selection Score-Ranked Compounds

Compound	Rank (Dock6)	Rank (Vina)	Δ Rank*
S12-2-33	1	4	3
S12-2-50-23	3	13	10
S12-2-50-37	6	10	4
S12-37	9	5	4
S12-37-37	10	14	4
S10-17	11	9	2
S10-24	12	12	0
S10-06	15	1	14

*) Spearman rank correlation analysis demonstrated a statistically significant moderate positive correlation between DOCK6 and AutoDock Vina–derived Selection Scores ($\rho = 0.474$, $p < 0.001$), indicating partial directional agreement in compound prioritization across the two independent docking platforms.

Table 5. Algorithmic characteristics of docking engines used for consensus docking

Docking Engine	Search Algorithm	Scoring Function	Mathematical Representation	Key Characteristics
DOCK6	Anchor-and-Grow incremental construction	Grid-based van der Waals and electrostatic scoring	(E_{grid} = E_{vdW} + E_{elec})	Interaction energies between ligand and receptor are precomputed on a 3D grid surrounding the binding site. Ligand fragments are placed using sphere matching and incrementally grown within the pocket.
AutoDock Vina	Iterated Local Search (ILS) with BFGS local optimization	Empirical scoring function combining steric, hydrophobic, hydrogen bonding, and torsional terms	(E = w_1G_1 + w_2G_2 + w_3H_{bond} + w_4H_{phob} + w_5N_{rot})	Combines stochastic global search with local optimization to explore ligand conformations. The scoring function integrates steric complementarity, hydrogen bonding, hydrophobic interactions, and torsional penalties.

Table 6. ADMET Prediction Analysis

Ligands	MW	#H-bond acceptors	#H-bond donors	MR	TPSA	WLOGP	BBB	LD_{50} (mg/kg)	Ames Mutagenicity	Score ADMET
original ligan 8f4s_(5a)	381.39	10	6	92.73	208.65	-2.38	No	971.65	0.99	0.778
S12-2-33	331.41	3	2	87.71	67.43	1.41	Yes	892.14	0.29	1
S12-2-50-23	418.08	4	2	82.74	67.43	2	Yes	1722.4	0.34	1
S12-2-50-37	312.72	4	2	82.74	67.43	2	Yes	967.14	0.32	1
S12-37	288.34	3	2	87.55	67.43	1.35	Yes	925.24	0.35	1
S12-37-37	306.33	4	2	87.51	67.43	1.91	Yes	920.61	0.3	1
S10-17	294.3	4	2	80.38	88.5	2.62	No	658.54	0.76	0.945
S10-24	308.33	4	2	85.19	88.5	3.01	No	690.13	0.76	0.945
S10-06	296.28	5	4	77.94	119.73	2.02	No	447.71	0.93	0.945
Nirmatrelvir	531.88	9	1	128.08	117.45	3.59	No	81.49	0.08	0.222
Indinavir	499.53	8	3	125.68	131.4	1.6	No	1837.48	0.25	0.667
Ensitrelvir	602.58	12	4	150.43	213.36	2.21	No	921.94	0.11	0.361
Lopinavir	157.1	4	2	32.91	88.84	-0.57	No	1530.14	0.04	0.472
Molnupiravir	628.8	5	4	187.92	120	3.57	No	2187.4	0.68	0.667
Ritonavir	329.31	8	4	76.02	143.14	-1.65	No	824.17	0.25	0.722
Remdesivir	720.94	7	4	197.82	202.26	5.6	No	331.12	0.1	0.417
Favipiravir	613.79	7	4	182.62	118.03	1.63	No	2000.16	0.33	0.667

ADMET Prediction Analysis

The predicted ADME and toxicity profiles of the fifteen top-ranked derivatives are summarized in Table 6. Most S12-series derivatives demonstrated favorable pharmacokinetic and toxicity parameters compared with the reference antiviral drugs. All prioritized S12 derivatives fulfilled Lipinski's Rule of Five, with molecular weights ranging from 288 to 418 Da, appropriate numbers of hydrogen bond donors (2) and acceptors (3–4), and moderate molar refractivity values. These characteristics are consistent with properties commonly associated with oral bioavailability and membrane permeability[36].

The majority of S12 derivatives exhibited TPSA values of 67.43 $Å^2$ and moderate lipophilicity (WLOGP 1.35–2.29), supporting favorable passive diffusion potential. In contrast, several reference drugs, including remdesivir and ensitrelvir, displayed substantially higher molecular weights and TPSA values, which may limit passive permeability. Predicted blood–brain barrier (BBB) permeability was positive for most S12 derivatives, whereas S10-series compounds and all reference drugs were predicted as BBB-negative. In this context, BBB positivity is interpreted as an indicator of favorable membrane permeability rather than central nervous system targeting[37].

Toxicity prediction indicated moderate LD_{50} values for S12 derivatives (approximately 700–1800 mg/kg), consistent with low acute toxicity risk. Ames mutagenicity probabilities ranged from 0.29 to 0.37 for most S12 compounds, remaining below the commonly applied threshold of 0.5, suggesting a low predicted mutagenic potential [38]. In contrast, S10-06 and S10-17 exhibited higher Ames probabilities (0.93 and 0.76, respectively), which contributed to slightly reduced overall ADMET scores.

The calculated ADMET scores reflected these differences. Most S12 derivatives achieved a score of 1.0, indicating fulfillment of all predefined criteria. S10-series compounds (S10-17, S10-24, and S10-06) showed slightly lower scores (0.945), primarily due to higher Ames values. Reference antiviral drugs displayed more variable and generally lower ADMET scores (0.222–0.722), largely influenced by high molecular weight, elevated TPSA, or predicted permeability limitations[34].

Overall, five compounds of the S12 derivatives demonstrated more balanced pharmacokinetic and toxicity profiles within the defined screening criteria. While these predictions remain computational and require experimental validation, the ADMET evaluation supports the prioritization of selected S12 compounds for further in vitro or in vivo validation.

However, final compound selection was not based solely on ADMET performance but also considered binding interaction consistency and cross-platform ranking stability. Among the evaluated compounds, three derivatives (S12-2-33, S12-37, and S10-24) were identified as prioritized candidates, demonstrating a balanced profile in binding interactions, predicted ADMET properties, and consensus docking stability.

CONCLUSION

This study implemented a structure-based virtual screening strategy to evaluate dihydropyrimidinone (DHPM) and chromene derivatives as potential inhibitors of SARS-CoV-2 NSP16 by targeting its cryptic allosteric pocket. Integration of docking analysis, consensus cross-platform validation, and ADMET-based selection scoring enabled systematic prioritization of candidate compounds within the designed derivative library.

Three prioritized compounds demonstrated consistent interaction patterns within the validated cryptic pocket and maintained stable ranking positions across independent docking engines. In addition, their predicted pharmacokinetic and toxicity profiles fulfilled the predefined ADMET criteria, supporting their suitability for further investigation.

It is important to emphasize that all findings in this study are based on computational predictions. Docking scores and ADMET evaluations provide relative estimations and do not fully capture the complexity of biological systems, including protein dynamics, solvent effects, and in vivo pharmacokinetics. Therefore, the identified compounds should be considered as preliminary candidates that require further experimental validation to confirm their biological activity and safety profiles.

ACKNOWLEDGEMENTS

Thank you for the consultants, colleagues for the insightful discussions, constructive input and all the support provided by the Research Center for Bio-Molecule Engineering (BIOME) Universitas Airlangga and Institute of Tropical Disease (RC-GERID) Universitas Airlangga. This Research is financially supported by the Indonesian Ministry of Higher Education through Research Funds (DRTPM) 2023 in the

platform Doctoral Research Grant for 1-year study based on No. 114/ E5/PG.02.00.PL/ 2023 and received no external funding.

REFERENCES

1. Angius F, Puxeddu S, Zaimi S, et al. SARS-CoV-2 Evolution : Implications for Diagnosis , Treatment , Vaccine Effectiveness and Development. 2025;2(March 2020):1-38.
2. Soares VC, Moreira IBG, Dias SSG. SARS-CoV-2 Infection and Antiviral Strategies: Advances and Limitations. *Viruses*. 2025;17(8). doi:10.3390/v17081064
3. Yan D, Yan B. Viral target- and metabolism-based rationale for combined use of recently authorized small molecule COVID-19 medicines: molnupiravir, nirmatrelvir and remdesivir. 2024;37(4):726-738. doi:10.1111/fcp.12889.Viral
4. Batool S, Chokkakula S, Jeong JH, Baek YH, Song M suk. Heliyon SARS-CoV-2 drug resistance and therapeutic approaches. *Heliyon*. 2025;11(2):e41980. doi:10.1016/j.heliyon.2025.e41980
5. Adriaty, D; Suwito HPN. Antiviral Potential of Dihydropyrimidinone, Chromene and Chalcone Derivatives Against SARS-CoV-2. *Trends Sci*. Volume 23,.
6. Adriaty D, Suwito H, Nyoman N, et al. In Vitro Antiviral Activity and Molecular Docking Analysis of Dihydropyrimidinone, Chromene and Chalcone Derivatives Against SARS-. 2026;23(December 2019):1-18.
7. Adriaty D, Suwito H, Nurrohman AI, Nyoman N, Puspaningsih T. Virtual Screening of Dihydropyrimidinone and Chromene Derivatives for Potential Dual Inhibition of SARS-CoV-2 Proteases Mpro and PLpro ABSTRACT : 2025;18(September):4425-4434. doi:10.52711/0974-360X.2025.00635
8. Omer EA, Abdelfatah S, Riedl M, Meesters C, Hildebrandt A, Efferth T. Coronavirus Inhibitors Targeting nsp16. Published online 2023:1-13.
9. Nencka R, Silhan J, Klima M, et al. Critical Reviews and Perspectives Coronaviral RNA-methyltransferases : function ,. 2022;50(2):635-650. doi:10.1093/nar/gkab1279
10. Misra A, Rahisuddin R, Parihar M, Harris RS, Martinez-sobrido L. Article Structural insights into the assembly and regulation of 2 0 - O RNA methylation by SARS-CoV- II Structural insights into the assembly and regulation of 2 0 - O RNA methylation. Published online 2025:1027-1039. doi:10.1016/j.str.2025.03.009
11. Inniss NL, Kozic J, Li F, et al. Discovery of a Druggable, Cryptic Pocket in SARS-CoV-2 nsp16 using Allosteric Inhibitors. 2024;9(10):1918-1931. doi:10.1021/acsinfecdis.3c00203.Discovery
12. Amalina I, Puspaningsih NNT, Suwito H. In Silico analysis of pyrimidine derivatives as potential antibacterial agents. *AIP Conf Proc*. 2023;2536(1):50004. doi:10.1063/5.0121466
13. Dharmapalan BT, Biswas R, Sankaran S, et al. Inhibitory Potential of Chromene Derivatives on Structural and. *Viruses*. 2022;2022(14):2656.
14. Patrick GL. *An Introduction to Medicinal Chemistry*. 7th ed. Oxford University Press; 2023.
15. Castro-González LM, Alvarez-Idaboy JR, Galano A. Computationally Designed Sesamol Derivatives Proposed as Potent Antioxidants. *ACS omega*. 2020;5(16):9566-9575. doi:10.1021/acsomega.0c00898
16. López-lópez E, Cerda-garcía-rojas CM, Medina-franco JL. Consensus Virtual Screening Protocol Towards the Identification of Small Molecules Interacting with the Colchicine Binding Site of the Tubulin-microtubule System Research Article. 2023;2200166:1-8. doi:10.1002/minf.202200166
17. Blanes-mira C, Fern P, Andr J De, Ferrer-montiel A, Fern G, Fern A. Comprehensive Survey of Consensus Docking for High-Throughput Virtual Screening. Published online 2023.
18. Trott O, Olson AJ. AutoDock Vina: improving the speed and accuracy of docking with a new scoring function, efficient optimization, and multithreading. *J Comput Chem*. 2010;31(2):455-461. doi:10.1002/jcc.21334
19. Maladan Y, Krismawati H, Martogi H, Hutapea L. A new Mycobacterium leprae dihydropteroate synthase variant (V39I) from Papua , Indonesia. 2019;(October 2018):1-14. doi:10.1016/j.heliyon.2019.e01279
20. Maier JA, Martinez C, Kasavajhala K, Wickstrom L, Hauser KE, Simmerling C. ff14SB: Improving the Accuracy of Protein Side Chain and Backbone Parameters from ff99SB. *J Chem Theory Comput*. 2015;11(8):3696-3713. doi:10.1021/acs.jctc.5b00255
21. Allen WJ, Balius TE, Mukherjee S, et al. DOCK 6: Impact of new features and current docking performance. *J Comput Chem*. 2015;36(15):1132-1156. doi:10.1002/jcc.23905
22. Coumar MS. Molecular Docking for Computer-Aided Drug Design. *Mol Docking Comput Drug Des*. Published online 2021. doi:10.1016/c2019-0-04960-6
23. Galano A, Castro-gonza LM, Rau J. Computationally Designed Sesamol Derivatives Proposed as Potent Antioxidants. Published online 2020. doi:10.1021/acsomega.0c00898
24. Palacio-Rodríguez K, Lans I, Cavasotto CN, Cossio P. Exponential consensus ranking improves the outcome in docking and receptor ensemble docking. *Sci Rep*. 2019;9(1):5142. doi:10.1038/s41598-019-41594-3
25. Daina A, Michielin O, Zoete V. SwissADME: A free web tool to evaluate pharmacokinetics, drug-likeness and medicinal chemistry friendliness of small molecules. *Sci Rep*. 2017;7:1-13. doi:10.1038/srep42717
26. Martin TM. User's Guide for T. E. S. T. (Toxicity Estimation Software Tool) Version 5.1. Published online 2020. https://www.epa.gov/chemical-research/toxicity-estimation-software-tool-test
27. Adriana P, Castan R, Gabriel E, Felipe L, Galano A. Chalcone Derivatives with a High Potential as Multifunctional Antioxidant Neuroprotectors. Published online 2022. doi:10.1021/acsomega.2c05518
28. Alturaifi TM, Scofiel GE, Wang S, Liu P. A database of steric and electronic properties of heteroaryl substituents. Published online 2025:1-12.
29. Khasimbi S, Ali F, Manda K, Sharma A, Chauhan G, Wakode S. Dihydropyrimidinones Scaffold as a Promising Nucleus for Synthetic Profile and Various Therapeutic Targets: A Review. *Curr Org Synth*. 2021;18(3):270-293. doi:10.2174/1570179417666201207215710
30. Omer EA, Abdelfatah S, Shahhamzehei N, et al. Identification of nsp16 inhibitors of SARS -CoV-2, SARS -CoV-1 and MERS-CoV from FDA-approved drugs using in silico and in vitro methods. *Biomed Pharmacother*. 2025;189:118246. doi:10.1016/j.biopha.2025.118246
31. Kumar S, Kumar S. Chapter 6 - Molecular Docking: A Structure-Based Approach for Drug Repurposing. In: Roy K, ed. *In Silico Drug Design*. Academic Press; 2019:161-189. doi:https://doi.org/10.1016/B978-0-12-816125-8.00006-7
32. Coumar MS. *Molecular Docking for Computer-Aided Drug Design*.
33. Vittorio S, Lunghini F, Morerio P, et al. Addressing docking pose selection with structure-based deep learning: Recent advances, challenges and opportunities. *Comput Struct Biotechnol J*. 2024;23:2141-2151. doi:https://doi.org/10.1016/j.csbj.2024.05.024
34. Pérez-González A, Castañeda-Arriaga R, Guzmán-López EG, Hernández-Ayala LF, Galano A. Chalcone Derivatives with a High Potential as Multifunctional Antioxidant Neuroprotectors. *ACS omega*. 2022;7(43):38254-38268. doi:10.1021/acsomega.2c05518
35. Agu PC, Afiukwa CA, Orji OU, et al. Molecular docking as a tool for the discovery of molecular targets of nutraceuticals in diseases management. *Sci Rep*. 2023;13(1):13398. doi:10.1038/s41598-023-40160-2

36. Lipinski CA, Lombardo F, Dominy BW, Feeney PJ. Experimental and computational approaches to estimate solubility and permeability in drug discovery and development settings. *Adv Drug Deliv Rev*. 2001;46(1-3):3-26. doi:10.1016/s0169-409x(00)00129-0

37. Vallianatou T, Giaginis C, Tsantili-Kakoulidou A. The Impact of Physicochemical and Molecular Properties in Drug Design: Navigation in the ``Drug-Like'' Chemical Space. In: Vlamos P, Alexiou A, eds. *GeNeDis 2014*. Springer International Publishing; 2015:187-194.

38. Riyadi PH, Romadhon, Sari ID, et al. SwissADME predictions of pharmacokinetics and drug-likeness properties of small molecules present in Spirulina platensis. *IOP Conf Ser Earth Environ Sci*. 2021;890(1). doi:10.1088/1755-1315/890/1/012021

Cite this article: Dinar A, Hery S, Ni N T P. Design and Virtual Screening of Dihydropyrimidinone and Chromene-Based Derivatives as Potential SARS-CoV-2 NSP16 Methyltransferase Inhibitors. Pharmacogn J. 2026;18 (2): 171-180.